Journal of ELECTRONIC MATERIALS, Vol. 48, No. 8, 2019
https://doi.org/10.1007/s11664-019-07269-5

Crystal Structures and Phase-Transitions Analysis of the Double Perovskites $Sr_2Co_{1-x}Ni_xTeO_6$ (x = 0.25, 0.5 and 0.75) Using X-ray Powder Diffraction, Raman and Infrared Spectroscopy

A. ZARAQ,[1,4] B. ORAYECH,[2,5] J.M. IGARTUA,[3] and A. EL BOUARI[1]

1.—Laboratory of Physico Chemistry of Applied Materials (LPCMA), Faculty of Sciences Ben M'Sik, University Hassan II Casablanca, 20702 Casablanca, Morocco. 2.—Maxam, Technology Center Energetic Materials, Carretera N-623 km 28, 09141 Quintanilla Sobresierra, Burgos, Spain. 3.—Fisika Aplikatua II Saila, Zientzia eta Teknologia Fakultatea, Euskal Herriko Unibertsitatea, P.O.Box 644, 48080 Bilbao, Spain. 4.—e-mail: assmaa.zaraq@gmail.com. 5.—e-mail: orayech@gmail.com

The reaction between the complexes of double perovskite formula $Sr_2Co_{1-x}Ni_xTeO_6$ in different stoichiometric proportions (x = 0.25, 0.5 and 0.75) have been processed in polycrystalline form by solid– state reaction mode in air. Based on the Rietveld refinements of x-ray powder diffraction data, the crystal structures and phase transitions, at room temperature of this double perovskite series are reported. The materials crystallize in a monoclinically distorted perovskite structure (the two compositions with x = 0.5 and 0.75 belong the to $I2/m$ space group, while the composition with x = 0.25 crystallize in $P2_1/n$ space group). We found a good agreement between the lattice parameters of this series and those of the two materials Sr_2CoTeO_6 and Sr_2NiTeO_6 with x = 0 and 1, respectively. The linear evolution of crystalline parameters proves the realization of the Vegard Law. The effect of the partial substitution of Co by Ni was also seen in the spectra of Raman and infrared, where a band shift was observed with increased nickel content.

Key words: $Sr_2Co_{1-x}Ni_xTeO_6$ double perovskites oxides, x-ray powder diffraction, phase transition, Rietveld refinements, Raman and infrared spectroscopy, crystal structure

INTRODUCTION

The basic simple perovskite with general formula ABO_3 has cubic symmetry, where A is typically a large, low oxidation state cation and B is a smaller cation (normally a transition metal) that can adopt octahedral coordination. The simple perovskite structure is composed of a three dimensional network of regular corner-shared MO_6 octahedra. Historically the octahedral site (M cation) is designated as the B-site. In the ideal case, the B-site cations are at the center of the octahedral with A cations centrally located in the body center of the cube formed by eight corner-shared octahedral (twelve coordination).[1,2]

The introduction of two transition metal ions at the B-site and A-sites of the perovskite structure leads to other symmetries and gives rise to a subclass of compounds which are referred to as double perovskites with stoichiometry $A'A''B'B''O_6$.[3]

The crystalline structure of the $A_2B'B''O_6$ stoichiometry is based on the manner in which the (B′ and B″) cations are dispersed at the octahedral sites, the degree of cation inversion, the size and the electronic structure of the change in the metal cations B′ and B″.[4,5] Therefore, many previous

(Received June 21, 2018; accepted May 2, 2019; published online May 17, 2019)

reviews have focused on the impact of the systematic change in size, charge and electronic configuration of (B′ and B″) cations on the B-site arrangement.[6–8] Recently, crystallographic investigations of the same materials have shown that the ordered structure is based on the charge contrast between B′ and B″ and is probably to be formed if this difference is above or equal to 2.[9–11] The concept of Tolerance Factor (t) was introduced for the first time by Goldschmidt in 1926 and is commonly used to analyze the structure–property relationships of ceramics with perovskite crystal structure (ABO_3). The tolerance factor for perovskites materials is a geometric parameter that measures the deviation of the structure from the ideal compact stacking position of atoms and is also used to indicate the likely stability of perovskite compounds.[12] Based on ionic radiation and assuming a spherical model where the anions and cations are concerned, the tolerance factor of the double perovskites can be expressed by the equation $t = \frac{\bar{r}_{(A)}+r_O}{\sqrt{2}\left(\bar{r}_{(B',B'')}+r_O\right)}$, where $\bar{r}_{(A)}$ is the average ionic radius of the A cations, $\bar{r}_{(B',B'')}$ the mean ionic radius of the B′ and B″ cations and r_O is the ionic radius of the oxygen, which are tabulated by Shannon.[13]

As mentioned previously, the doubles perovskites oxides form an important class of materials characterized by structural distortions from a typical cubic structure ($Fm\ \bar{3}m$, No. 225) to another symmetry more distorted than the cubic. The structural distortions are produced by deformations as well as rotations of BO_6 and $B'O_6$ octahedral with respect to the crystallographic axes of the material in order to allow the size of the A-site cations.

On the one hand, several studies have proven that the double perovskite materials were identified by phase transition behavior with structure type $A_2B'B''O_6$ under the effect of temperature and/or pressure.[14–16] Many researches were carried out on double perovskites with hexavalent cations, such as Sb, Nb, Mo, Re, W, Ta, and Te.[17–19] The p-block elements such as tellurium can be strongly stabilized in the B-sites of the perovskite structure, presenting the required spherical symmetry and adequate ion size.[20]

On the other hand, the physical properties of double perovskites materials, magnetic and electrical for instance, are influenced by the phase transition behavior. Hence, their technological importance becomes more valuable, allowing this prototype to emerge in a variety of materials applications used to store energy; specifically in electronic devices and sensors thanks to their electrical and/or piezoelectric properties. These fascinating materials could also have applications as magnetic memory components, electrode and electrolyte materials for fuel cells and ceramic electrolytes in lithium solid state batteries.[21–27]

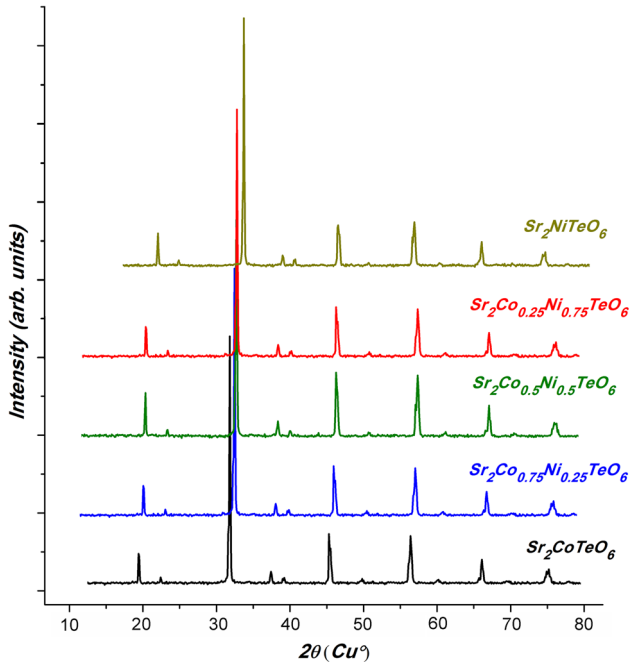

Fig. 1. X-ray powder diffraction patterns for the series of double perovskite $Sr_2Co_{1-x}Ni_xTeO_6$ with (x = 0, 0.25, 0.5, 0.75 and 1).

Table I. Tolerance factor calculated using the ionic radii suggested by Shannon radius

Compound	Tolerance factor
Sr_2CoTeO_6	0.9858
$Sr_2Co_{0.75}Ni_{0.25}TeO_6$	0.9886
$Sr_2Co_{0.5}Ni_{0.5}TeO_6$	0.9920
$Sr_2Co_{0.25}Ni_{0.75}TeO_6$	0.9954
Sr_2NiTeO_6	0.9989

In recent years, double perovskites containing cobalt with $A_2CoB'O_6$ formula have produced a big interest in the field of solid materials. The Sr_2CoTeO_6 oxide has been studied by many researchers, and they have reported that this material has a monoclinical structure with the space group $P2_1/n$. These findings were confirmed with x-ray diffraction investigations.[28,29] From the 1940s, Sr_2NiTeO_6 oxide has been of great importance in the scientific community. The first studies focus on its properties, for example, they were used like a dielectric material for capacitors.[30] The symmetry of the crystal of Sr_2NiTeO_6 is $I2/m$.[31]

As mentioned herein above, the crystal structure of both extremes Sr_2CoTeO_6 and Sr_2NiTeO_6 have been studied previously. However, to our knowledge, at the time of writing this report, no previous work has been reported on the series $Sr_2Co_{1-x}Ni_xTeO_6$ with (x = 0.25, 0.5 and 0.75). Herein, we report for the first time the room temperature crystal structures of the new doubles perovskites $Sr_2Co_{1-x}Ni_xTeO_6$ with (x = 0.25, 0.5 and 0.75) using x-ray

powder diffraction (XRPD), Raman and infrared spectroscopy. On the other hand, the structural phase transition at room temperature and with the cobalt content changed is also analyzed.

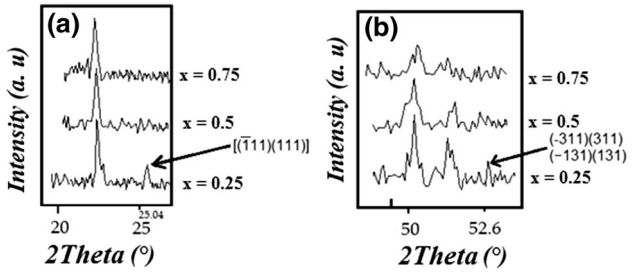

Fig. 2. Selected (2θ) intervals for the three compositions of the $Sr_2Co_{1-x}Ni_xTeO_6$ series with (x = 0.25, 0.5 and 0.75) determined the disappearance of the reflections that characterizes the primitive peaks $h + k + l = 2n + 1$ of the usual $P2_1/n$ space group,(a) The [(1̄11)(111)] reflections located around 25.04° and 25.06°,(b) The [(–311)(311); (–131)(131)] reflections located around 52.57° and 52.90°.

EXPERIMENTAL TECHNIQUE

Sample Preparation

Different compositions of the series $Sr_2Co_{1-x}Ni_xTO_6$ with (x = 0.25, 0.5 and 0.75) were synthesized by conventional high-temperature solid-state reaction from stoichiometric amounts of TeO_2 (99.9%) and $Ni(NO_3)_2.6H_2O$ (99.9%), $CoCO_3$(99.98%) and $SrCO_3$(99.9%), according to the following reaction:

$$2SrCO_3 + (1-x)CoCO_3 + x\,Ni(NO_3)_2, 6H_2O + TeO_2 \rightarrow Sr_2Co_{1-x}Ni_xTeO_6 + 3-x\,CO_2 \uparrow + 3x\,H_2O \uparrow + 2x\ NH_3 \uparrow + (8x-1)/2O_2 \uparrow \text{ with } (x = 0.25,\ 0.5 \text{ and } 0.75).$$

All compounds were used as received from Sigma to Aldrich. The samples were heated in air, in alumina crucibles, at progressively higher temperatures 300°C/6 h, 600°C/12 h, 800°C/12 h, 900°C/24 h, 1000°C/24 h and 1100°C/24 h with periodic intermediate grinding. The purity of the obtained materials was confirmed using XRD. A minor

Table II. Refined parameters for $Sr_2Co_{1-x}Ni_xTeO_6$ with (x = 0.25, 0.5 and 0.75) at room temperature from x-ray powder diffraction

Composition	x = 0	x = 0.25 [PW]	x = 0.50 [PW]	x = 0.75 [PW]	x = 1
Wavelength (Å)	kα1 = 1.540560	kα1 = 1.540560	kα1 = 1.540560	kα1 = 1.540560	kα1 = 1.540560
2θ step scan increment	0.010	0.010	0.010	0.010	0.010
(°)	10–108	10–80.5	10–80.5	10–80.5	10–100
2θ range (°)	FullProf	FullProf	FullProf	FullProf	FullProf
Program	− 0.05197	0.14858	0.15705	0.22891	− 0.02843
Zero point (2θ°)	0.29307	0.6088	0.30627	0.34347	0.30897
Pseudo–Voigt function					
PV = $\eta L + (1-\eta) G$	U = 0.085708	U = 0.033135	U = 0.018613	U = 0.359381	U = 0.083092
Caglioti parameters	V = − 0.013058	V = − 0.007323	V = 0.008129	V = − 0.122570	V = − 0.014735
	W = 0.024828	W = 0.006729 48	W = 0.007390 46	W = 0.030111 43	W = 0.035106
No. of refined parameters	Monoclinic	Monoclinic	Monoclinic	Monoclinic	Monoclinic
Crystal system	$P2_1/n$	$P2_1/n$	$I2/m$	$I2/m$	$I2/m$
Space group	5.6437(2)	5.6410(2)	5.6341(2)	5.6300 (2)	5.6166(1)
a (Å)	5.6096(2)	5.6045(2)	5.5976(2)	5.5933(2)	5.5807(1)
b (Å)	7.9271(2)	7.9164(2)	7.9035(2)	7.9020(2)	7,8797(1)
c (Å)	90.059(2)	90.066(3)	90.066(2)	89.9729(2)	90.048(2)
β (°)	250.96(2)	250.280(2)	249.55(2)	247.94(2)	246.97(10)
V (Å^3)	2	2	2	2	2
Z	4	5	5	5	4
Atom number	2.40	2.72	1.88	3.68	4.00
RB	4.20	6.23	3.31	4.16	5.00
RF	3.20	4.94	4.93	2.89	9.20
RP	4.00	6.40	6.43	3.67	13.10
RWP	1.50	1.07	1.08	1.24	2.1
X^2					

pw Present work.

impurity (around 1%) of Sr_3TeO_6 was observed for the composition $Sr_2Co_{0.75}Ni_{0.25}TeO_6$.

XRPD Measurements

The final products of chemical reactions were characterized by x-ray powder diffraction at room temperature with an Analytical X'Pert-PRO (θ–2θ) diffractometer, using Cu-Ka radiation (45 kV, 40 mA). The data were collected from 13 to 80° 2θ, through steps of 0.01 (2θ). The refinements of the structures were achieved by the Rietveld method employing the FullProf program.[32] The peaks of the x-ray powder diffraction (XRPD) lines was defined using a pseudo–Voigt function, considering the background is adapted with a fifth order polynomial. The structural refinement by the Rietveld method of the observed x-ray powder diffraction (XRPD) data is begun with scale and the others parameters are refined according to this order: scale factor, zero shift, the cell parameters, background, atomic positions, asymmetry parameters, and the parameters of thermal agitation of the atoms.

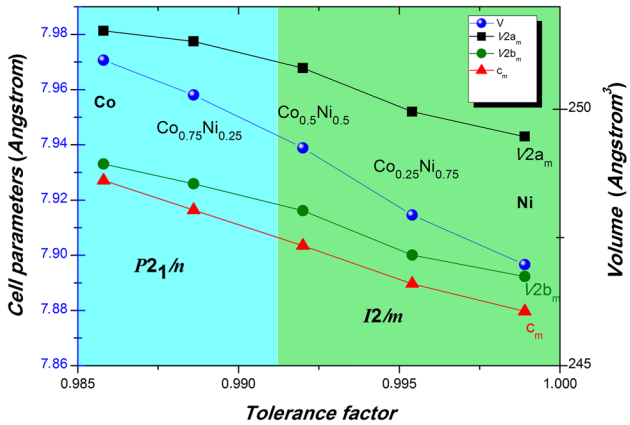

Fig. 3. Variation of the lattice parameters and the volume of the unit cell as a function of tolerance factor of the $Sr_2Co_{1-x}Ni_xTeO_6$ series with (x = 0, 0.25, 0.5, 0.75 and 1). The a and b values of cells have been multiplied by $\sqrt{2}$ for clarity.

Raman and Infrared Spectroscopy

The Raman spectra was reported on DXR2 Raman Microscope. The spectral range is 3500–100 cm^{-1} captured with a single exposure of the CCD for avoiding stitching artifacts, a laser type diode pumped, solid state (DPSS) (Spectra-Physics, 600 nm, 8 mW), and an optical system (with spectral resolution 2 cm^{-1} FWHM). All measurements were carried out at room temperature.

The infrared spectra was recorded in the form of KBr pellets in the wave number range 4000–400 cm^{-1} using a Mattson 7000 spectrometer, then they are treated using the Win-IR software.

RESULTS AND DISCUSSION

Indexing and Refinement of Structures by the Rietveld Method

The x-ray diffractograms obtained at room temperature of the mixtures of the double perovskite series $Sr_2Co_{1-x}Ni_xTeO_6$ with (x = 0, 0.25, 0.5, 0.75 and 1) are shown in Fig. 1. These patterns demonstrated that the peak positions of the x-ray powder

Table III. Refined atomic positions (x, y, z) and thermal isotropic factors (Biso) of $Sr_2Co_{1-x}Ni_xTeO_6$with (x = 0.25, 0.5 and 0.75), from XRPD data at RT

		$Sr_2Co_{1-x}Ni_xTeO_6$ (x = 0.25, 0.5 and 0.75)		
Composition	**Atom**	**Atomic coordinate**	**B (Å²)**	**Occupancy**
x = 0.25 ($P2_1/n$)				
	Sr	(0.5074, 0.0066, 0.2493)	1.6900	2.0000
	Co/Ni	(0, 0, 0)	2.7000	0.75/0.25
	Te	(0, 0, ½)	2.0200	1.0000
	O (1)	(0.9450, -0.0410, 0.7430)	1.8000	2.0000
	O (2)	(0.2550, 0.2980, 0.9820)	1.8000	2.0000
	O (3)	(0.7290, 0.2430, 0.0290)	2.0000	2.0000
x = 0.5 ($I2/m$)				
	Sr	(0.5010, 0.0000, 0.7505)	1.8600	2.0000
	Co/Ni	(½, ½, 0)	2.4800	0.5/0.5
	Te	(0, 0, 0)	2.0600	1.0000
	O (1)	(0.0440, 0.0000, 0.7610)	2.9000	2.0000
	O (2)	(0.2370, 0.2360, 1.0280)	1.9000	4.0000
x = 0.75 ($I2/m$)				
	Sr	(0.4900, 0.0000, 0.7513)	1.5000	2.0000
	Co/Ni	(½,½, 0)	0.7000	0.25/0.75
	Te	(0, 0, 0)	1.4500	1.0000
	O (1)	(0.045, 0.0000, 0.740)	0.8000	2.0000
	O (2)	(0.208, 0.256, 1.026)	1.1000	4.0000

diffraction (XRPD) lines are identical to other double perovskite phases.[28,29,31]

To index the x-ray diffraction patterns of this series, we used the computer program Dicvol.[32] This double perovskite series $Sr_2Co_{1-x}Ni_xTeO_6$ (x = 0.25, 0.5 and 0.75) is isostructural with Sr_2CoTeO_6 and Sr_2NiTeO_6 crystallizing in the space groups $P2_1/n$ and $I2/m$, respectively.[29,31]

The tolerance factor values of this series were calculated from the following equation:

$$t = \frac{\frac{r_A}{2} + r_O}{\sqrt{2}\left(\frac{r'_B + r_{B''}}{2} + r_O\right)},$$

where $r_A, r_{B'}$ and $r_{B''}$, are the averaged ionic radii of the Sr, Co, Ni and the Te cations in the double perovskite series $Sr_2Co_{1-x}Ni_xTeO_6$. For completeness, the tolerance factor is secured for the extreme compounds Sr_2CoTeO_6 and Sr_2NiTeO_6. The values of tolerance factor collected in Table I prove, on the one hand, that the room-temperature structures of the compounds should not be cubic, and, on the other hand, that the $Sr_2Co_{0.75}Ni_{0.25}TeO_6$ compound is more distorted than $Sr_2Co_{0.5}Ni_{0.5}TeO_6$ and $Sr_2Co_{0.25}Ni_{0.75}TeO_6$ compounds, respectively.

The XRPD patterns show that the peaks are split, meaning that the unit cells of these materials are fairly distorted with respect to the cubic symmetry. As shown in Fig. 2, the characteristic primitive peaks [($\bar{1}$ 11) (111)] and [(−311) (311) (131) (−131)], $h + k + l = 2n + 1$ of the $P2_1/n$ space group are observed for the composition $Sr_2Co_{0.75}Ni_{0.25}TeO_6$. The first ($2\theta$) region includes the reflections [($\bar{1}$ 11) (111)] located around 25.04° and 25.06°, the second region contains the reflections [(− 311) (311); (− 131) (131)] located around 52.57° and 52.90°. However for the compositions with (x = 0.5 and 0.75) these primitive reflections are not present. Figure 2 shows the selected (2θ) intervals (25.04°–25.06°) and (52.57°–52.90°) for the three compositions of the $Sr_2Co_{1-x}Ni_xTeO_6$ (x = 0.25, 0.5 and 0.75) series. To find the suitable space group of the compounds with (x = 0.25, 0.5 and 0.75), structural refinements have been carried out using both models of $P2_1/n$ and $I2/m$ symmetries. The results show good reliability factors for the refinement of the $Sr_2Co_{0.75}Ni_{0.25}TeO_6$ composition with the monoclinic $P2_1/n$ space group. While for the other compositions $Sr_2Co_{0.5}Ni_{0.5}TeO_6$ and $Sr_2Co_{0.25}Ni_{0.75}TeO_6$, the refinements showed better fitting with the $I2/m$ structural model and good reliability factors (Table II).

Based on the results showed herein above, the monoclinic space group $P2_1/n$ has been attributed to the composition $Sr_2Co_{0.75}Ni_{0.25}TeO_6$. While for $Sr_2Co_{0.5}Ni_{0.5}TeO_6$ and $Sr_2Co_{0.25}Ni_{0.75}TeO_6$, the monoclinic space group $I2/m$ was assigned. This means that the series $Sr_2Co_{1-x}Ni_xTeO_6$ (x = 0.25, 0.5 and 0.75) suffers a structural phase transition at room temperature as nickel content increases.

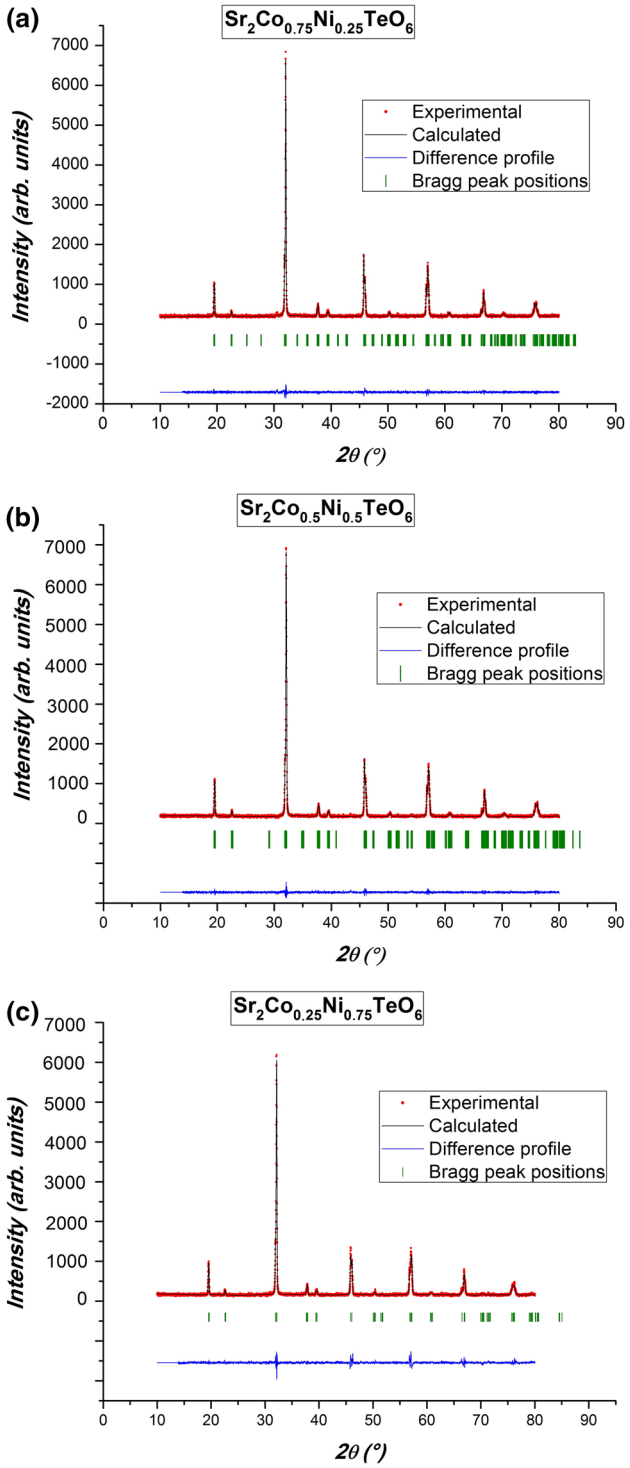

Fig. 4. Experimental (symbols) and calculated (line) x-ray profiles for the final Rietveld plots of, (a) $Sr_2Co_{0.75}Ni_{0.25}TeO_6$, (b) $Sr_2Co_{0.5}Ni_{0.5}TeO_6$ and (c) $Sr_2Co_{0.25}Ni_{0.75}TeO_6$.

Figure 3 shows the evolution of the cell parameters as the content of Ni increases. The cell parameters of Sr_2CoTeO_6 and Sr_2NiTeO_6 are included for completeness. This evolution shows that the unit cell of the series $Sr_2Co_{1-x}Ni_xTeO_6$ gets smaller as the tolerance factor increases, or, in other words, as

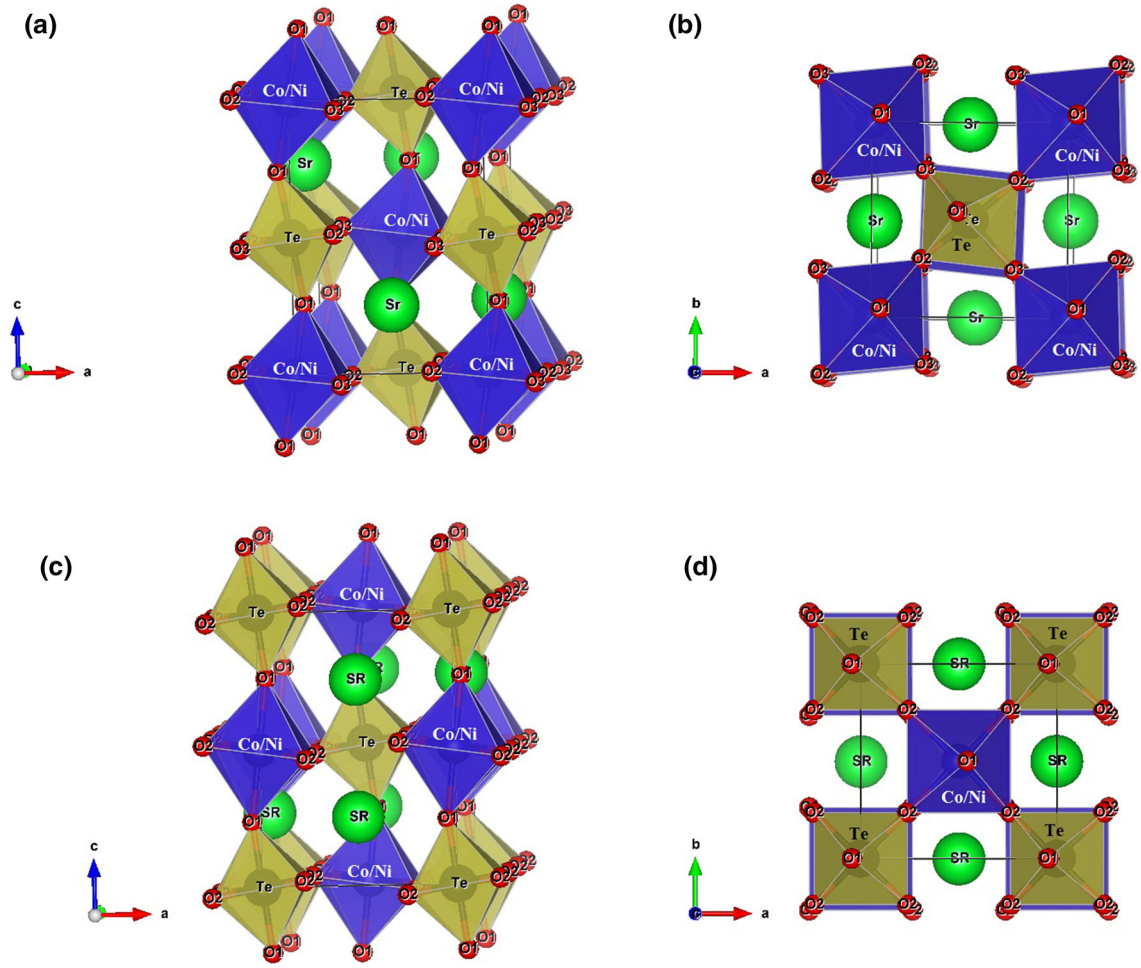

Fig. 5. Polyhedral views of the monoclinical structure of $Sr_2Co_{1-x}Ni_xTeO_6$ double perovskite with (x = 0.25, 0.5 and 0.75) at room temperature generated by VESTA: (a) and (b) of (x = 0.25), (a) is [110] view of anti-phase rotation of the $(Co/Ni)O_6$ and TeO_6 octahedral networks according to the tilt system $a^-b^-c^+$, and (b) [001] view of in-phase. (c) and (d) crystal structure of the composition (x = 0.5), projected along the *b*-axis and *c*-axis, respectively. Sr (big spheres), Co, Ni and Te (spheres inside the octahedral), O (small spheres).

the value $r_{Co2+} + r_{Ni2+}$ gets smaller. It is worth noting that the cell parameters of both extremes Sr_2CoTeO_6 and Sr_2NiTeO_6 follow perfectly this evolution. This linear evolution indicates that the $Sr_2Co_{1-x}Ni_xTeO_6$ series verifies Vegards's law.[33]

The refinement of the x-ray powder diffraction patterns of $Sr_2Co_{0.75}Ni_{0.25}TeO_6$ was carried out using the structural model of the monoclinic $P2_1/n$ reported in the study already done on material Sr_2CoTeO_6,[29] in this model Sr^{2+}, Co^{2+}/Ni^{2+} and Te^{6+} atoms are set at 4e (x, y, z), 2a (0, 0, 0) and 2b (0, 0, ½) sites, respectively (see Table III).

Regarding the compositions (x = 0.5, 0.75), the refinement of the x-ray powder diffraction patterns was achieved from the model as indicated in the study already done on material Sr_2NiTeO_6,[31] in this exemplary of symmetry, the Sr^{2+}, (Co^{2+}/Ni^{2+}) and Te^{6+} atoms are arranged at 4i (x, 0, z), 2d (½, ½, 0) and 2a (0, 0, 0) sites, respectively. There are two crystallographically distinct oxygen molecules; (O (1) 4i (x, 0, z) and O (2) 8j (x, y, z)), present in the unit cell. The refined atomic positions and the isotropic atomic displacement parameters (Biso) for the series $Sr_2Co_{1-x}Ni_xTeO_6$ (x = 0.25, 0.5 and 0.75) in the monoclinical symmetry with more crystallographic details are listed in Table III. The last plots of the observed and calculated profiles at ambient temperature for the compound with (x = 0.25) that crystalized in $P2_1/n$ space group, also for the two compounds with (x = 0.5 and 0.75) modeled the in $I2/m$ space group, are recorded individually in Fig. 4.

Description of the Structure

The monoclinical structures of the materials $Sr_2Co_{1-x}Ni_xTeO_6$ with (x = 0.25, 0.5 and 0.75, generated by VESTA program,[34] are shown in Figs. 5 and 6. These figures demonstrate that the sites B and B′ containing the cations (Co/Ni) and Te, respectively, are coordinated by six oxygens in a distorted octahedral arrangement. The oxygen atoms connect the octahedral in all three directions.

The objective from this part of our study is to present more details about these monoclinic

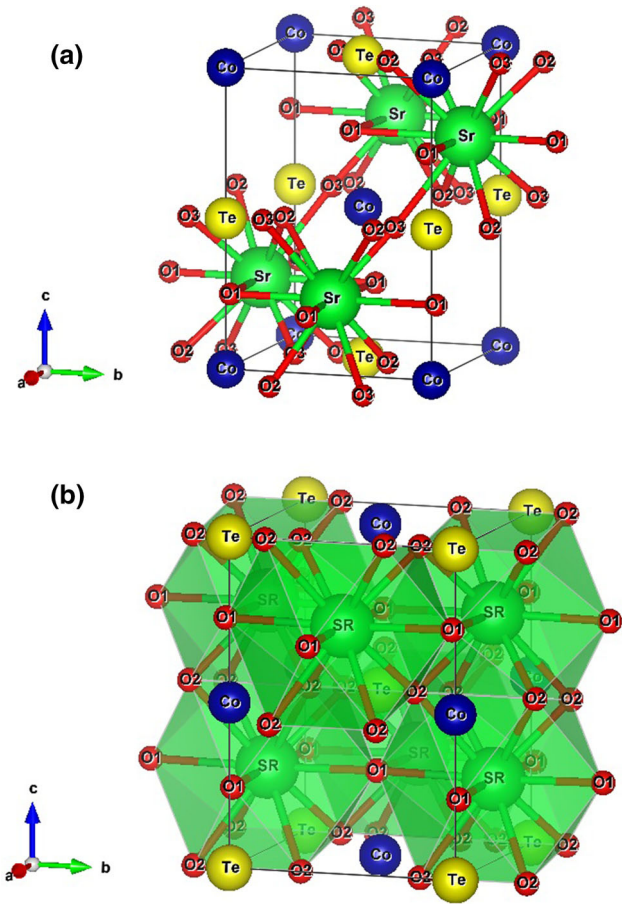

Fig. 6. The polyhedral SrO_{12} environment of (a) $Sr_2Co_{0.75}Ni_{0.25}TeO_6$ and (b) $Sr_2Co_{0.5}Ni_{0.5}TeO_6$.

crystalline structures. In Tables IV and V, we selected the bond distances and angles for our double perovskite compositions. The bond distance qualities are in great contrast with the aggregate of Shannon's ionic radii of cations; $(Ni^{2+}/Co^{2+}) + O^{2-}$ = 2.08 Å; $Te^{6+} + O^{2-}$ = 1.91 Å.

From the values of the atomic distances stated in Table IV and also from the Fig. 5, we observed that the octahedral $(Co/Ni)O_6$ and TeO_6 are slightly distorted. The perovskite structure crystallizing with $P2_1/n$ symmetry is anticipated by the tilt system $(a^-b^-c^+)$ (see Fig. 5b), according to Glazer notation.[35] About the crystalline structure defined by the $I2/m$ model is characterized by an amplitude of rotation which is zero along the axes [100] and a tilting of the octahedral $(Co/Ni)O_6$ and TeO_6 along the axes [010]p and [001]p of the original perovskite, the rotations around the two axes being anti-phase (-) $(a^0b^-b^-)$ (see Fig. 5(d)), as initially suggested by Glazer.[35] The average (Co/Ni)-O and Te-O distances are identical to those found in related double perovskite compounds (Sr_2CoTeO_6 and Sr_2NiTeO_6).

The octahedral $(Co/Ni)O_6$ and TeO_6 of the composition (x = 0.25) are associated by O (1) and O (2) along a and b axis, and by O (3) along c-axis. The tilt of the octahedral is seen from the three bond angles [(Co/Ni)-O(1)-Te (168.8°), (Co/Ni)-O(2)-Te (165.2°) and (Co/Ni)-O(3)-Te (155.6°)]. About the two compositions (x = 0.5 and 0.75), the $(Co/Ni)O_6$ and TeO_6 octahedral are associated by O (1) along c-axis, and by O (2) along a and b axis, the incline of the octahedral for these both compositions is discovered from the two bond angles [Co/Ni-O (1)-Te (165.7°) and Co/Ni-O (2)-Te (167.2°)] for the composition (x = 0.5), [Co/Ni-O (1)-Te (163.8°) and Co/Ni-O (2)-Te (167.3°)], for the arrangement 0.75.

Table IV. Main bond distances (Å) and selected angles (°) for $Sr_2Co_{1-x}Ni_xTeO_6$ (x = 0.25, 0.5, and 0.75)

Composition Space group	x = 0.25 $P2_1/n$	x = 0.5 $I2/m$	x = 0.75 $I2/m$
Co/NiO6 Octahedra			
Co/Ni-O (1)	2.07(3)	2.08(2)	2.10(2)
Co/Ni-O (2)	2.09(14)	2.10(17)	2.13(2)
Co/Ni-O (3)	2.06(15)		
Average distance	2.07	2.09	2.11
Predicted distance	2.09	2.10	2.13
TeO_6 Octahedra			
Te-O (1)	1.91(3)	1.90(2)	1.90(2)
Te-O (2)	1.93(15)	1.89(4)	1.87(2)
Te-O (3)	1.98(14)		
Average distance	1.94	1.89	1.88
Predicted distance	1.98	1.92	1.90
O (1)-Co/Ni-O (2)	94(8)	91(14)	91(14)
O (1)-Co/Ni-O (3)	99(8)	90.5(11)	98.1(16)
O (2)-Co/Ni-O (3)	93(11)		
O (1)-Te-O (2)	96(8)	91.3(16)	90(2)
O (1)-Te-O (3)	97(8)	91.4(13)	97.4(18)
O (2)-Te-O (3)	91(11)		
Co/Ni-O (1)-Te	172.1(13)	165.7(10)	163.8(10)
Co/Ni-O (2)-Te	164(6)	167.2(7)	167.3(9)
Co/Ni-O (3)-Te	158(6)		

Strontium (Sr^{2+}) atoms form an environment of twelve coordination polyhedral (SrO_{12} cuboctahedra) with bond lengths (Sr-O) between 2.3 and 3.13 Å and an average value 2.8 Å (see Table V). For the compositions crystallizing in the space group $P2_1/n$, the faces of the polyhedral SrO_{12} are linked by the oxygen O (2) and O (3) along the c axis, whereas in the plane (ab) these polyhedral are connected by four oxygen atoms O (1). Concerning the compositions crystallizing in the space group $I2/m$, the binding of the faces of the polyhedral SrO_{12} is made by oxygen O (1) along the c axis. On the plane (ab), the bond of these polyhedral is made by four oxygen atoms type O (2).

When the nickel value increases in the monoclinic compositions, we observed important reductions of the distances Te-O from 1.94 Å to 1.89 Å and 1.88 Å (see Table IV).

Group–Theory Analysis of Vibrational Raman and Infrared Active Modes

To have more structural information about the nature of bonding in this series of double perovskite

$Sr_2Co_{1-x}Ni_xTeO_6$ (x = 0.25, 0.5 and 0.75), in this part of the work, Raman and IR spectroscopic studies were achieved. In the first we have used group theory to classify the vibratory states of our double perovskite series. As the $Sr_2Co_{1-x}Ni_xTeO_6$ (x = 0.25, 0.5 and 0.75) series of double perovskite structure crystallized in the both monoclinic symmetries ($P2_1/n$ and $I2/m$ space groups) at ambient conditions, in Table VI we have cited the activity of the different modes possible by these space groups.[36]

The analysis of the site symmetry group of the compounds $Sr_2Co_{1-x}Ni_xTeO_6$ (x = 0.25, 0.5 and 0.75) that modeled in the two space group ($I2/m$, C2 h (2/m) point group) and ($P2_1/n$, $P2_1/c$ (No. 14)) conduce to the next irreducible representations:

$$T(P2_1/n) = 12\mathrm{Ag}\,(R) + 12\mathrm{Bg}\,(R) + 3\mathrm{Au}\ (\mathrm{IR}) + \mathrm{Au}\,(\mathrm{ac}) + 2\mathrm{Bu}\,(\mathrm{ac}) + 36\mathrm{Bu}\,(\mathrm{IR})$$
$$T(I2/m) = 7\mathrm{Ag}\,(\mathrm{R}) + 5\mathrm{Bg}\,(\mathrm{R}) + 7\mathrm{Au}\,(\mathrm{IR}) + 11\mathrm{Bu}\,(\mathrm{IR}) + \mathrm{Au}\,(\mathrm{ac}) + 2\mathrm{Bu}\,(\mathrm{ac})$$

In which the symbols stands for: R-Raman active modes, IR-infrared active modes, ac-acoustic modes.

The analysis of the site symmetry group (see Table VI) shows that there are 24 Raman active modes, announced by ν(Raman) = 12Ag + 12Bg, that ought to be noticed for the monoclinic compo-

Table V. Sr-O bond distances (Å) of $Sr_2Co_{1-x}Ni_xTeO_6$ with (x = 0.25, 0.5 and 0.75)

x = 0.25 ($P2_1/n$)	x = 0.5 and 0.75 ($I2/m$)	x = 0.25 ($P2_1/n$)	x = 0.5 ($I2/m$)	x = 0.75 ($I2/m$)
Sr-O1	Sr-O1	2.64(4)	2.58(3)	2.47(4)
Sr-O1	Sr-O1	3.01(4)	3.06(3)	3.18(4)
Sr-O1	Sr-O1	2.77(10)	2.812(3)	2.814(4)
Sr-O1	Sr-O1	2.85(10)	2.812(3)	2.814(4)
Sr-O2	Sr-O2	2.95(5)	2.96(2)	2.89(5)
Sr-O2	Sr-O2	3.03(5)	2.64(2)	2.89(5)
Sr-O2	Sr-O2	2.61(5)	2.64(2)	2.89(5)
Sr-O2	Sr-O2	2.65(5)	2.96(2)	2.89(5)
Sr-O3	Sr-O2	2.52(4)	2.66(2)	2.72(5)
Sr-O3	Sr-O2	2.56(4)	2.97(2)	2.74(5)
Sr-O3	Sr-O2	3.13(4)	2.97(2)	2.74(5)
Sr-O3	Sr-O2	3.13(4)	2.66(2)	2.72(5)

Table VI. Factor group analysis for $Sr_2Co_{1-x}Ni_xTeO_6$ for the range (x = 0.25, 0.5 and 0.75) at room temperature

Symmetry	Atom	Site	A_g	A_u	B_g	B_u	Modes
$P2_1/n$	Te	2b		6		6	$M = 6A_u + 6B_u$
	Co/Ni	2a		6		6	$M = 6A_u + 6B_u$
	Sr	4e	3	6	3	6	$M = 3A_g + 6A_u + 3B_g + 6B_u$
	O (1)	4e	3	6	3	6	$M = 3A_g + 6A_u + 3B_g + 6B_u$
	O (2)	4e	3	6	3	6	$M = 3A_g + 6A_u + 3B_g + 6B_u$
	O (3)	4e	3	6	3	6	$M = 3A_g + 6A_u + 3B_g + 6B_u$
	$T_{Total} = 48A + 48B = 96$ $T_{acustic} = A_u + 2B_u$						
	$T_{Raman} = 12A_g + 12B_g$ $T_{Infrared} = 36A_u + 36B_u$						
$I2/m$	Te	2a		1		2	$M = 1A_u + 2B_u$
	Co/Ni	2d		1		2	$M = 1A_u + 2B_u$
	Sr	4i	2	1	1	2	$M = 2A_g + A_u + B_g + 2B_u$
	O (1)	4i	2	1	1	2	$M = 2A_g + A_u + B_g + 2B_u$
	O (2)	8j	3	3	3	3	$M = 3A_g + 3A_u + 3B_g + 3B_u$
	$T_{Total} = 14A + 16B = 30$ $T_{acustic} = A_u + 2B_u$						
	$T_{Raman} = 7A_g + 5B_g$ $T_{Infrared} = 7A_u + 11B_u$						

sitions with the space group $P2_1/n$, and twelve active modes ν(Raman) = 7Ag (R) + 5Bg (R) should be observed for the compositions crystallizing with the centered monoclinic space group $I2/m$.[37]

Raman Spectroscopy Study for the $Sr_2Co_{1-x}Ni_xTeO_6$ Perovskite Double Series

Figure 7 presents the Raman spectra for the $Sr_2Co_{1-x}Ni_xTeO_6$ series with (x = 0.25, 0.5 and 0.75) recorded at room temperature. The evolution of the spectra is correlated with those found in the double perovskite literature. They are also in agreement with those obtained for materials $Ba_{2-x}Sr_xMgTeO_6$ ($0 \le x \le 2$).[37] The Raman modes observed and the assignment are given in Table VII.

Raman spectrum analysis has shown that most bands in our system are small; there are only three bands and they are located around ($\sim$ 412 cm^{-1}; 550 cm^{-1} and $\sim$ 750 cm^{-1}).

The Raman modes observed in this $Sr_2Co_{1-x}Ni_xTeO_6$ double perovskite series with (x = 0.25, 0.5 and 0.75) can be classified into three general families of network vibrations[37]:

- At wave numbers below < 350 cm^{-1}, concerns the translation of Sr^{2+} cations, as well as a translation and rotation mode of TeO_6 octahedral.
- The region 350–500 cm^{-1} relates to the bending modes of O-(Te)-O.
- At wave numbers greater than 550 cm^{-1}, refers to the (Te)-O elongation modes.

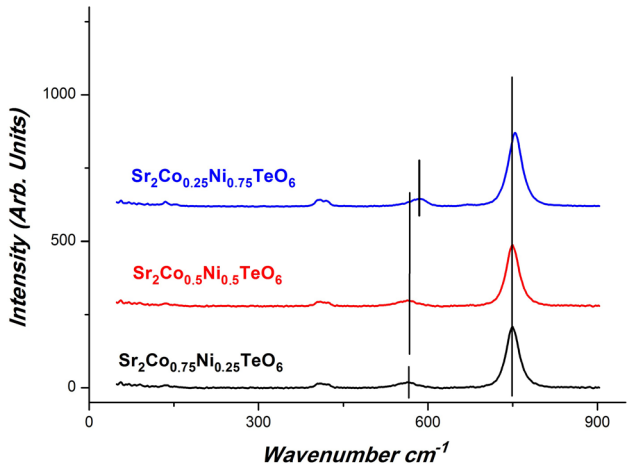

Fig. 7. Raman spectra of $Sr_2Co_{1-x}Ni_xTeO_6$ with (x = 0.25, 0.5 and 0.75) recorded at ambient conditions.

We are interested only in the internal modes of the double perovskite structure corresponding to the octahedron ($B^{6+}O_6$by reason of the 1: 1 order attributes of this type of materials, that interposed powerfully the (TeO_6) octahedral and faintly the other octahedral ((Co/Ni)O_6).[38]

The investigation of the spectra demonstrates a slight modification in the Raman modes of the series $Sr_2Co_{1-x}Ni_xTeO_6$ with (x = 0.25, 0.5 and 0.75). We put the vertical lines on the Raman spectrum bands to signal the small change in modes produced in these double perovskite series. In Fig. 8a, b and c we present the evolution of Raman mode values according to the composition x, demonstrating the monoclinic phase transition from $P2_1/n$ symmetry to $I2/m$ symmetry due to the expansion of the amount of nickel and confirming the Rietveld refinements studies.

Infrared Spectroscopy Study

Figure 9 shows the infrared (IR) spectra of the $Sr_2Co_{1-x}Ni_xTeO_6$ series prepared with (x = 0.25, 0.5 and 0.75) at room temperature. Infrared modes observed are given in Table VIII. The most impressive component evident in this Fig. 9 is the immense proximity between the bands of the infrared and Raman spectra, especially at the level of the band around the recurrence of 750 cm^{-1}. The bandwidths are identical on the whole arrangement of compounds. The positions and intensities of the bands are generally comparable starting from one compound to another, but a little variation in the modes is obtained with the expansion of nickel in the compounds. According to this increase of nickel, the characters of the structure fluctuate fundamentally starting with one compound then onto the next. The sharp bands present in these spectra are demonstrative of an arranged diffusion of Te.[38]

The increasing of the amount of nickel in the double perovskites series $Sr_2Co_{1-x}Ni_xTeO_6$ produced a decrease in cell parameters. This modification in the concentration of Ni and Co cations also

Table. VII. Raman shift (in cm^{-1}) for the observed modes in $Sr_2Co_{0.75}Ni_{0.25}TeO_6$, $Sr_2Co_{0.5}Ni_{0.5}TeO_6$ and $Sr_2Co_{0.25}Ni_{0.75}TeO_6$

ν ($Sr_2Co_{0.75}Ni_{0.25}TeO_6$)	ν ($Sr_2Co_{0.5}Ni_{0.5}TeO_6$)	ν ($Sr_2Co_{0.25}Ni_{0.75}TeO_6$)	Assignment
407	411	414	ν_5
560	575	587	ν_2
748	760	775	ν_1

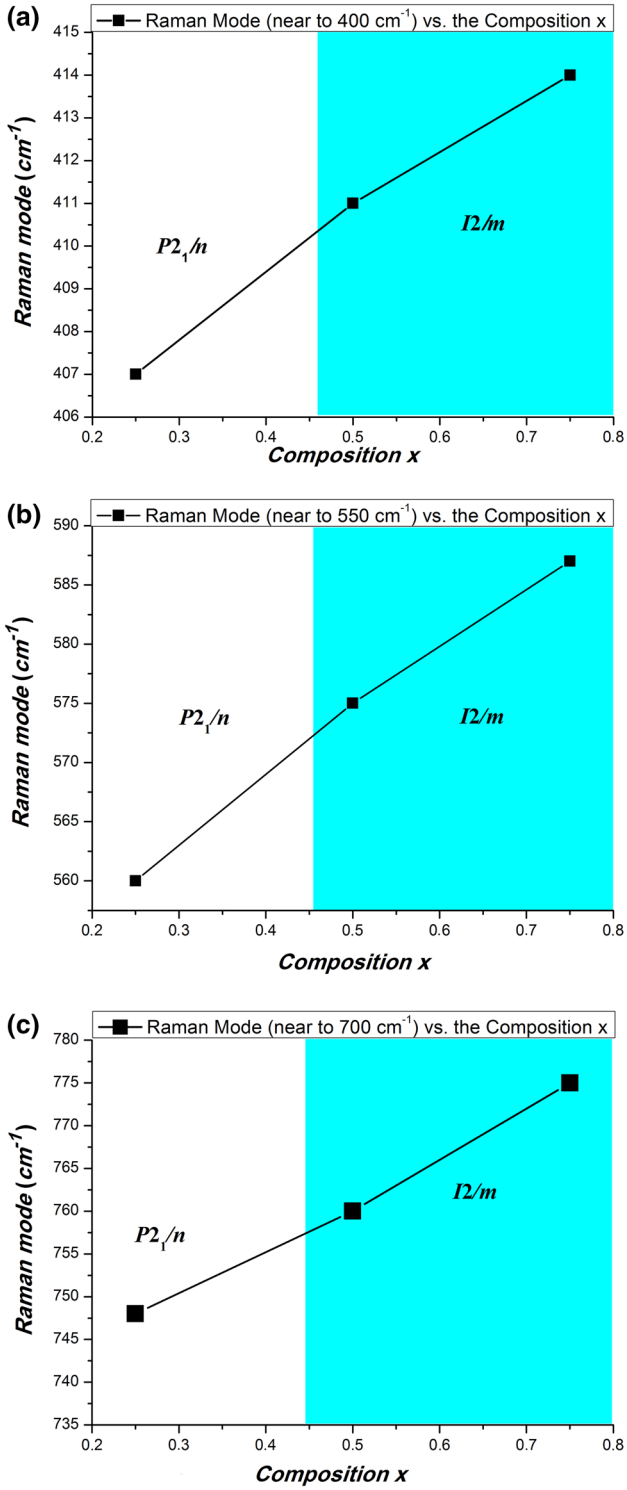

Fig. 8. Raman modes of $Sr_2Co_{1-x}Ni_xTeO_6$ depending on the composition x, (a) Raman Mode (near to 400 cm^{-1}), (b) Raman Mode (near to 550 cm^{-1}) and (c) Raman Mode (near to 700 cm^{-1}).

affects the arrangement of the octahedral ((Co/Ni)-O) and (Te-O) in the structure. From the Raman and infrared spectra, we observed a bit change in

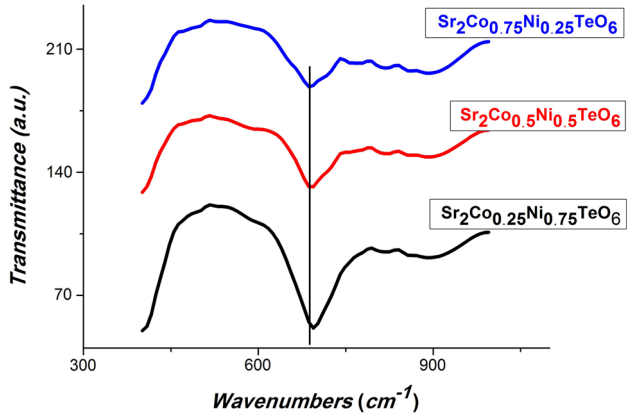

Fig. 9. The infrared spectra of $Sr_2Co_{1-x}Ni_xTeO_6$ with (x = 0.25, 0.5 and 0.75) compounds.

the frequency of Raman mode around 750 cm^{-1}, confirming the phase transition behavior induced by the extension of the Ni cations.

To illustrate this consequence, and based on studies already done on this type of material [38] the frequency ν_1 situated around 750 cm^{-1} is considered as corresponding to the Te-O bonding energies. The data already show in Table IV and V, indicating that the distances of the tellurium atom in connection to the oxygens (Te-O) are reducing. Then again, the distances of (cobalt and nickel) in relation to the oxygens atoms (Co/Ni)-O are growing. This effect, expands the Te-O bonding energy, and therefore produces an increase of the mode frequency located around 750 cm^{-1}.

CONCLUSION

In the present research, utilizing the x-ray powder diffraction (XRPD), Raman and infrared (IR) spectroscopy, we have performed a description of the crystal structure of $Sr_2Co_{1-x}Ni_xTeO_6$ (x = 0.25, 0.5 and 0.75) double perovskite oxides, and we have confirmed the monoclinical distortion (from the primitive symmetry $P2_1/n$ to the centered symmetry $I2/m$) induced by the expansion of the nickel component, at room temperature. The analysis via Rietveld refinements noticed that the monoclinical distortion happened in the midst of the two compositions (x = 0.25 and 0.5). We chose the monoclinical symmetry $I2/m$ as a space group of the composition with (x = 0.5) by reason of the good obtained values for the reliability factor. The Raman and infrared spectra of ordered double perovskites $Sr_2Co_{1-x}Ni_xTeO_6$ have been registered and analyzed at room temperature. These analyzes justified the phase transition revealed by a change of the mode to a high frequency value in the Raman and infrared spectra.

Table VIII. Infrared displacement (in cm^{-1}) for the modes observed in the $Sr_2Co_{1-x}Ni_xTeO_6$ series

$Sr_2Co_{1-x}Ni_xTeO_6$			
v ($Sr_2Co_{0.75}Ni_{0.25}TeO_6$)	v ($Sr_2Co_{0.50}Ni_{0.50}TeO_6$)	v ($Sr_2Co_{0.25}Ni_{0.75}TeO_6$)	Assignment
680	680	684	v_1

ACKNOWLEDGMENTS

The authors would like to acknowledge University Hassan II, Casablanca, Morocco, for their support. We are grateful to Engineers (in Service Centrale d'Analyse (CSA) de l'Unités d'Appui Technique à la Recherche Scientifique (UATRS)" CNRS- Rabat, Morocco) for technical assistance.

REFERENCES

1. R.S. Roth, *J. Res. Natl. Bur. Stand.* 58, 75 (1957).
2. M. Ochi, I. Yamada, K. Ohgushi, Y. Kusano, M. Mizumaki, R. Takahashi, S. Yagi, N. Nishiyama, T. Inoue, and T. Irifune, *Inorg. Chem.* 52, 3985 (2013).
3. M.C. Knapp and P.M. Woodward, *J. Solid State Chem.* 179, 1076 (2006).
4. M.T. Anderson, K.B. Greenwood, G.A. Taylor, and K.R. Poeppelmeier, *Prog. Solid State Chem.* 22, 197 (1993).
5. Yu.E Smirnov, T.D. Smirnova, and I.A. Zvereva, *Rus. J. Gen. Chem.* 75, 1359 (2005).
6. R. Mukherjee, B. Ghosh, S. Saha, C. Bharti, and T.P. Sinha, *J. Rare Earths.* 32, 334 (2014).
7. T. Yang, T. Perkisas, J. Hadermann, M. Croft, A. Ignatov, and M. Greenblatt, *J. Solid State Chem.* 183, 2689 (2010).
8. S. Zhao, K. Yamamoto, S. Iikubo, S. Hayase, and T. Ma, *J. Phys. Chem. Solids* 117, 117 (2018).
9. T. Sugahara, M. Ohtaki, and K. Suganuma, *J. Asian Ceram. Soc.* 1, 282 (2013).
10. P.A. Kumar, S. Ivanov, C. Ritter, R. Vijayaraghavan, R. Mathieu, P. Nordblad, N. Sadovskaya, and D.D. Sarma, *J. Alloys Compd.* 693, 1096 (2017).
11. Z.W. Song and B.G. Liu, *Chin. Phys. B* 22, 047506 (2013).
12. V.M. Goldschmidt, *Naturwissenschaften* 14, 477 (1926).
13. R.D. Shannon, *Acta Crystallogr. A* 32, 751 (1976).
14. A. Zaraq, B. Orayech, A. Faik, J.M. Igartua, A. Jouanneaux, and A. El Bouari, *Polyhedron* 110, 119 (2016).
15. D.-D. Han, W. Gao, N.-N. Li, R.-L. Tang, H. Li, Y.-M. Ma, Q.-L. Cui, P.-W. Zhu, and X. Wang, *Chin. Phys. B* 22, 059101 (2013).
16. B. Orayech, L. Ortega-San-Martín, I. Urcelay-Olabarria, L. Lezama, T. Rojo María, I. Arriortua, and J.M. Igartua, *Dalton Trans* 44, 13716 (2015).
17. B. Orayech, A. Faik, and J.M. Igartua, *Polyhedron* 123, 265 (2017).
18. A. Faik, D. Orobengoa, E. Iturbe-Zabalo, and J.M. Igartua, *J. Solid State Chem.* 192, 273 (2012).
19. L.A. Baum, S.J. Stewart, R.C. Mercader, and J.M. Grenèche, *Hyperfine Interact.* 156, 157 (2004).
20. Y. Tang, R. Paria Sena, M. Avdeev, P.D. Battle, J.M. Cadogan, J. Hadermann, and E.C. Hunter, *J. Solid State Chem.* 253, 347 (2017).
21. K. Yamamura, M. Wakeshima, and Y. Hinatsu, *J. Solid State Chem.* 179, 605 (2006).
22. P.G.R. Achary, S.K. Dehury, and R.N.P. Choudhary, *J. Mater. Sci. Mater. Electron.* 29, 6805 (2018).
23. T. Zheng, J. Wu, D. Xiao, and J. Zhu, *Prog. Mater Sci.* 98, 552 (2018).
24. A. Khouidmi, H. Baltache, and A. Zaoui, *Chin. Phys. Lett.* 34, 076103 (2017).
25. Y. Huang, R. Dass, Z.-L. Xing, and J.B. Goodenough, *Science* 312, 254 (2006).
26. X. Zhang, Y. Jiang, X. Hu, L. Sun, and Y. Ling, *Electron. Mater. Lett.* 14, 147 (2018).
27. S.A. Dar, V. Srivastava, U.K. Sakalle, and V. Parey, *Eur. Phys. J. Plus* 133, 64 (2018).
28. M.S. Augsburger, M.C. Viola, J.C. Pedregosa, A. Muñoz, J.A. Alonso, and R.E. Carbonio, *J. Mater. Chem.* 15, 993 (2005).
29. L. Ortega-San Martin, J.P. Chapman, L. Lezama, J.S. Marcos, J. Rodrıguez-Fernandez, M.I. Arriortua, and T. Rojo, *J. Mater. Chem.* 15, 183 (2005).
30. YuN Venevtsev, E.D. Politova, and G.S. Zhdanov, *Ferroelectrics* 8, 489 (1974).
31. L. Ortega-San Martin, J.P. Chapman, G. Cuello, J. Gonzalez-Calbet, M.I. Arriortua, and T. Rojo, *Z. Anorg. Allg. Chem.* 631, 2127 (2005).
32. T. Roisnel and J. Rodríquez-Carvajal, *Mater. Sci. Forum* 378–381, 118 (2001).
33. A.R. Denton and N.W. Ashcroft, *Phys. Rev. A* 43, 3161 (1991).
34. K. Momma and F. Izumi, *J. Appl. Crystallogr.* 41, 653 (2008).
35. A.M. Glazer, *Acta Cryst.* A31, 756 (1975).
36. E. Kroumova, M.I. Aroyo, J.M. Perez-Mato, A. Kirov, C. Capillas, S. Ivantchev, H. Wondratschek, Phase Transit. 76 (2003) 155. http://www.cryst.ehu.es/.
37. Y. Tamraoui, B. Manoun, F. Mirinioui, R. Haloui, and P. Lazor, *J. Alloys Compd.* 603, 86 (2014).
38. A.P. Ayala, I. Guedes, E.N. Silva, M.S. Augsburger, M.C. del Viola, and J.C. Pedregosa, *J. Appl. Phys.* 101, 123511 (2007).